https://doi.org/10.5607/en24028
Exp Neurobiol. 2025 Apr;34(2):77-86.
pISSN 1226-2560 • eISSN 2093-8144

Original Article

Experimental Neurobiology

# Modeling Temporal Dependencies in Brain Functional Connectivity to Identify Autism Spectrum Disorders Based on Heterogeneous rs-fMRI Data

**Yaya Liu[1], Qiang Zhao[2*], Lishuang Zhao[3], Yanchun Liu[3] and Xiaoli Li[1]**

*[1]School of Computer Engineering, Hubei University of Arts and Science, Xiangyang 441053,*
*[2]School of Physics and Electronic Engineering, Hubei University of Arts and Science, Xiangyang 441053,*
*[3]College of Information Science and Technology, Bohai University, Jinzhou 121000, China*

Brain functional connectivity has shown promise for developing objective biomarkers for autism spectrum disorder (ASD). Although many imaging studies have demonstrated its potential, most have focused on static measurements. In this study, we explored the dynamic changes in functional connectivity over time to uncover potential temporal dependencies. These dynamic patterns were abstracted into high-level representations and used as predictors to identify individuals at risk of ASD. To achieve this, we employed a deep learning framework that combines attention mechanism with long short-term memory (LSTM) neural network. Experiments were conducted using heterogeneous resting-state functional magnetic resonance imaging (rs-fMRI) data from the Autism Brain Imaging Data Exchange (ABIDE) database. The resulting classification achieved an accuracy of 74.9% and precision of 75.5% under intra-site cross-validation, outperforming traditional classifiers such as support vector machines (SVM), random forests (RF), and single LSTM network. Further analyses demonstrated the robustness and generalizability of our model, with classification performance less affected by subjects' gender or age. The optimal model's weights revealed atypical temporal dependencies in the brain functional connectivity of individuals with ASD, highlighting the potential for these patterns to serve as biomarkers. Our findings underscore the importance of dynamic functional connectivity in understanding ASD and suggest that our deep learning framework could aid in the development of more accurate and reliable diagnostic tools for this disorder.

**Key words:** Autism spectrum disorder, Deep learning, Functional magnetic resonance imaging, Classification

## INTRODUCTION

Autism spectrum disorder (ASD) is a common developmental disorder characterized by significant deficits in social interaction and communication [1]. Currently, the clinical diagnosis of ASD relies predominantly on the observations of behavioral symptoms using standardized measures such as the autism behavior checklist (ABC) [2] and the childhood autism rating scale (CARS) [3]. However, these diagnostic methods can be subjective, with results varying based on clinicians' experience, and the process is often time-consuming. Given these limitations, there is a pressing need for more objective and precise diagnostic tools. Data-driven methods, which leverage advanced analytical techniques to identify potential patterns in large datasets, offer a promising avenue for improving the accuracy and efficiency of ASD diagnosis. By providing clinicians with additional, objective insights, these methods could enhance the precision of diagnostic outcomes and streamline the diagnostic process, ultimately benefiting individuals with ASD and their families.

In recent years, brain imaging techniques have advanced rapidly, prompting increasing interest in developing diagnostic methods for ASD based on brain imaging data [4-6]. One popular approach

Submitted October 20, 2024, Revised April 12, 2025,
Accepted April 15, 2025

*To whom correspondence should be addressed.
TEL: 86-176-2139-2600, FAX: 86-0710-3593152
e-mail: serene_shu@163.com

involves extracting brain connectivity information from resting-state functional magnetic resonance imaging (rs-fMRI) data to use as inputs for classifiers. For instance, Kong et al. [7] achieved a classification accuracy of 90.39% between typically developing (TD) individuals and patients with ASD by modeling preselected features of functional connectivity. Similarly, Guo et al. [8] explored low-dimensional representations of whole-brain connectivity, attaining a classification accuracy of 86.36%. And Chen et al. [9] demonstrated the potential of using functional connectivity at specific frequency bands, reporting a classification accuracy of 79.19%. Collectively, these studies have shown promising results in characterizing the pathophysiology of ASD through brain imaging data.

While imaging studies on brain connectivity have reported good accuracy in identifying individuals with ASD, they typically employ static measurements of functional connectivity. These static approaches, however, fail to adequately capture the temporal dependencies inherent in connectivity patterns. Recognizing that these temporal dependencies might contribute to the development of objective biomarkers for ASD and enhance our understanding of its underlying causes, we propose a novel method. This method focuses on the dynamic changes in connectivity over time to uncover potential temporal dependencies, thereby enabling more accurate distinction between TD individuals and patients with ASD.

To achieve accurate classification of individuals with ASD, we employed deep learning technology [10] in this study. As a currently popular and powerful approach, deep learning can automatically learn hierarchical representations of input data, which has led to promising results in identifying individuals with ASD. For instance, Deng et al. [11] developed a deep learning framework called the spatial-temporal transformer to investigate the spatial and temporal representations of rs-fMRI data, achieving a classification accuracy of 71.0%. Similarly, Heinsfeld et al. [12] utilized a deep neural network classifier based on autoencoders to discover inherent features in functional connectivity, reporting a classification accuracy of 70%. Eslami et al. [13] further demonstrated the potential of deep learning by characterizing rs-fMRI data using a joint learning procedure of autoencoder and perceptron, achieving an accuracy of 70.3%. These studies collectively highlight the significant potential of deep learning technology for screening individuals at risk of ASD.

In this study, we implemented an attention learning framework based on the long short-term memory (LSTM) neural network to model the temporal dependencies in brain functional connectivity. This approach aims to accurately differentiate between TD individuals and patients with ASD. To demonstrate the reproducibility and generalizability of our proposed classification model, we conducted experiments using heterogeneous rs-fMRI data from the Autism Brain Imaging Data Exchange (ABIDE) database.

## MATERIALS AND METHODS

### *Data preprocessing*

The ABIDE is an open-access repository that aggregates neuroimaging data from 1,112 subjects across 17 independent sites [14]. Of these, 1,102 subjects have complete labeling information. To standardize the sampling interval of the rs-fMRI data, we selected 634 valid subjects from 9 sites for our experiments, ensuring that each site had a repetition time (TR) of 2 seconds. These subjects span a broad spectrum of ages, symptom severities, and other relevant factors, which ensures that our dataset is representative of the broader ASD population. The inclusion of multiple sites helps to minimize site-specific biases and enhances the generalizability of our findings across different demographic and clinical subgroups. Table 1 provides detailed MRI hardware information for these sites, as well as key demographic information for the valid subjects. This information was compiled from the publicly available metadata and documentation of the ABIDE dataset. Among the se-

**Table 1.** MRI hardware and demographic data for selected sites

| SITE_ID | MRI hardware information | | | ASD | | TD | |
|---|---|---|---|---|---|---|---|
| | Vendor | Model | Magnetic field strength (Tesla) | Age avg (std) | Gender | Age avg (std) | Gender |
| CALTECH | Siemens | Prisma | 3.0 | 22.8 (6.8) | M 5, F 2 | 28.3 (11.2) | M 10, F 4 |
| CMU | Siemens | Prisma | 3.0 | 26.3 (4.9) | M 5, F 1 | 26.4 (4.3) | M 7, F 1 |
| NYU | Siemens | Trio Tim | 3.0 | 14.5 (7.0) | M 68, F 11 | 15.6 (6.1) | M 78, F 25 |
| SDSU | Siemens | Prisma | 3.0 | 14.6 (1.7) | M 10, F 1 | 13.9 (1.8) | M 12, F 6 |
| STANFORD | Philips | Achieva | 3.0 | 10.0 (1.6) | M 16, F 4 | 10.0 (1.6) | M 16, F 4 |
| TRINITY | Siemens | Prisma | 3.0 | 17.3 (3.6) | M 24, F 0 | 17.1 (3.9) | M 23, F 0 |
| UM | Siemens | Prisma | 3.0 | 13.8 (2.0) | M 58, F 10 | 15.3 (3.5) | M 59, F 18 |
| USM | Siemens | Trio Tim | 3.0 | 22.6 (7.7) | M 58, F 0 | 21.4 (7.6) | M 43, F 0 |
| YALE | GE | Signa HDxt | 3.0 | 12.6 (3.0) | M 19, F 8 | 12.7 (2.8) | M 20, F 8 |

M, male; F, female; avg, average; std, standard deviation.


https://doi.org/10.5607/en24028

lected subjects, there are 334 TD individuals and 300 patients with ASD. Notably, the number of male individuals with ASD exceeds that of females, which is consistent with established findings [15].

In this study, we utilized rs-fMRI data based on the Craddock 200 (CC200) atlas [16], which provides a functional parcellation of the brain into regions of interest (ROIs) with anatomical homology. This atlas enhances the interpretability of functional connectivity analyses by aligning them with well-defined anatomical regions and is widely used in ASD research, providing a standardized framework for comparing results across datasets. To address potential site variability and ensure consistency across sites, the rs-fMRI data were preprocessed using the configurable pipeline for the analysis of connectomes (CPAC) [17], a standardized preprocessing pipeline. The pipeline mainly included the following steps: (1) Slice time correction using AFNI's 3dTshift to account for the interleaved acquisition order of slices; (2) Motion correction using AFNI's 3dvolreg (two iterations) to correct for head movements during scanning; (3) Skull-stripping using AFNI's 3dAutomask to remove non-brain tissue; (4) Global mean intensity normalization to 10,000; (5) Nuisance regression to remove motion parameters, global mean signal, white matter signal, and cerebrospinal fluid signal; and (6) Band-pass filtering (0.01~0.1 Hz) to remove low-frequency drift and high-frequency physiological noise. More detailed information on the preprocessing pipeline and specific parameter settings are available in http://preprocessed-connectomes-project.org/.

To address potential site-related biases in our preprocessed data, we employed the ComBat method [18] for data harmonization. This method adjusts for systematic biases that may arise from variations in MRI scanners and protocols, ensuring that the data from different sites are comparable while preserving the biological signals of interest. Specifically, we used site information as the batch variable and included relevant covariates (i.e., age, gender, and diagnostic status) in the harmonization process. By doing so, we were able to mitigate the impact of site-specific differences on our analysis, thereby enhancing the robustness and generalizability of our findings.

Finally, we performed data segmentation using a sliding window approach [19], so as to capture the dynamic changes in functional connectivity over time. Specifically, we employed a window size of 30 seconds and a step size of 1 second. These parameters were chosen based on previous studies that have demonstrated their effectiveness in capturing temporal dependencies in rs-fMRI data while balancing temporal resolution and computational efficiency [20, 21]. This approach divided the preprocessed rs-fMRI data from each subject into a sequence of segments, with the length of each segment determined by the width of the sliding window. As a result, each segment reflects data acquisition over approximately 60 seconds, and the regular interval between two consecutive segments from the same subject is 10 seconds. Given the shortest duration of the preprocessed rs-fMRI data, a total of 24 segments, each of size $W \times M$, were extracted for each subject. Here, $W$ denotes the width of the sliding window, and $M$ represents the number of ROIs derived from the CC200 atlas.

### *Model implementation*

In the present study, we deployed an attention learning framework to accomplish the desired classification task. The framework primarily consists of two parts: feature extraction and attention learning. The feature extraction component focuses on characterizing the dynamic changes in brain functional connectivity over time, while the attention learning component emphasizes identifying discriminative connectivity patterns for accurate classification.

LSTM network is a special type of recurrent neural network (RNN) characterized by a chain structure of repetitive neural network modules [22]. Compared to traditional RNN, LSTM is capable of capturing intricate dependencies hidden in time series data. With this in mind, we utilized LSTM network for feature extraction and taken $G = \{G_1, G_2, \ldots, G_N\}$ as inputs to the network. Here, symbol $N$ represents the number of samples or subjects (i.e., 634). Let $S_i = \{S_{ij}\}_{j=1}^{24}$ denotes the sequence of segments derived from the $i$th subject, $G_i \in G$ could be considered as a mapping of $S_i$, achieved according to the following rules:

$$\rho_{ij}^{uv} = \frac{\mathrm{cov}\left(S_{ij}^u, S_{ij}^v\right)}{\sigma\left(S_{ij}^u\right) \cdot \sigma\left(S_{ij}^v\right)} \tag{1}$$

$$G_{ij} = \left(\rho_{ij}^{uv}\right)_{M \times M} \tag{2}$$

$$G_i = \left\{\eta_{triu}\left(G_{ij}\right)\right\}_{j=1}^{24} \tag{3}$$

where $S_{ij}^u$ and $S_{ij}^v$ are time series belonging to segment $S_{ij} = \{S_{ij}^k\}_{k=1}^{M}$, $\mathrm{cov}\left(S_{ij}^u, S_{ij}^v\right)$ indicates the covariance between $S_{ij}^u$ and $S_{ij}^v$, $\sigma\left(S_{ij}^u\right)$ and $\sigma\left(S_{ij}^v\right)$ imply the standard deviation of $S_{ij}^u$ and $S_{ij}^v$ respectively, and $\eta_{triu}\left(G_{ij}\right) \in R^{M*(M-1)/2}$ denotes a vector constructed with the upper triangular elements (excluding diagonal elements) of matrix $G_{ij}$.

Each module of LSTM network consists of four interactive components: the cell state, the forget gate, the input gate, and the output gate. Among these components, the cell state is the core of the network, responsible for storing important information, while the gates focus on filtering information. For the $j$th module, all three gates (forget, input, and output) perform operations using the current input vector $\eta_{triu}\left(G_{ij}\right) \in G_i$ and the output from the previous module $h_{i(j-1)}$ as inputs. Specifically, the forget gate $f_{ij}$ is calculated

as follows:

$$f_{ij} = \sigma\left(W_f \cdot \left[h_{i(j-1)}, \eta_{triu}\left(G_{ij}\right)\right] + b_f\right) \quad (4)$$

Here, parameters $W$, $b$ and $\sigma$ refer to the weight matrix, bias vector, and activation function of the current layer, respectively. The forget gate aims to determine what information needs to be discarded from the previous cell state $C_{i(j-1)}$. Meanwhile, the input gate $r_{ij}$ decides what new information from the input vector should be written to the current cell state $C_{ij}$. In other words, the information in the cell state is explicitly updated by the forget gate and the input gate. The corresponding formulations for the input gate and the current cell state are as follows:

$$r_{ij} = \sigma\left(W_r \cdot \left[h_{i(j-1)}, \eta_{triu}\left(G_{ij}\right)\right] + b_r\right) \quad (5)$$

$$C_{ij} = f_{ij} * C_{i(j-1)} + r_{ij} * \tanh\left(W_C \cdot \left[h_{i(j-1)}, \eta_{triu}\left(G_{ij}\right)\right] + b_C\right) \quad (6)$$

The output gate $o_{ij}$ makes a decision about the information to be exported from $C_{ij}$, which is considered as the output of the current module, i.e., $h_{ij} \in R^L$. Symbol $L$ here refers to the number of neurons in the LSTM network. The related formulations are as follows:

$$o_{ij} = \sigma\left(W_o \cdot \left[h_{i(j-1)}, \eta_{triu}\left(G_{ij}\right)\right] + b_o\right) \quad (7)$$

$$h_{ij} = o_{ij} * \tanh\left(C_{ij}\right) \quad (8)$$

Thus, the output of the network could be generated by aggregating the outputs from various modules and is denoted as $H_i = \{h_{ij}\}_{j=1}^{24}$. It represents the feature map of the sample $G_i$ based on the LSTM network. Considering the potential redundancy of information in the feature map, we deployed an autoencoder network layer above the LSTM for attention learning. This autoencoder contains one hidden layer and takes $H_i$ as input. The goal of the autoencoder network is to produce an attention distribution $A_i = \{a_{ij}\}_{j=1}^{24}$, which indicates the contribution of the feature map's information to accurate classification. The detailed formulation of $A_i$ is shown as follows:

$$A_i = softmax\left(W_A \cdot \gamma\left(H_i\right) + b_A\right) \quad (9)$$

where $\gamma$ represents the projection from the input layer to the hidden layer in the autoencoder network.

Subsequently, an operation as following formula was performed between $H_i$ and $A_i$, both of which have the same size. The resulting vector, which integrates the most informative features weighted by the attention distribution, was then fed into a softmax layer to predict the class label of the sample $G_i$. The possible values of this label are 0 or 1, corresponding to a patient with ASD or a TD individual, respectively. In summary, the attention learning framework essentially establishes a non-linear mapping process from input samples to predicted labels. The samples are represented as a sequence of segments, allowing the model to capture both static functional connectivity within local segments and dynamic changes across the global sequence.

$$att_i = \sum_{j=1}^{24} a_{ij} h_{ij} \quad (10)$$

Fig. 1 illustrates the architecture of the proposed attention learning model, which encompasses several key phases: data acquisition and segmentation, measurement of functional connectivity, vectorization, and training/testing. Initially, rs-fMRI data are acquired and segmented into a sequence of time windows to capture dynamic changes in brain activity over time. Functional connectivity is then measured within each segment, generating connectivity matrices that are subsequently transformed into feature vectors. These vectors serve as inputs for the attention learning model, which is trained and tested using intra-site cross-validation to assess its performance. This validation method could effectively reduce site-related variability, providing a robust measure of the model's generalization ability [23]. The training-to-testing sample ratio is set at 4:1, with five runs conducted to determine the experimental results.

The attention learning model was implemented and evaluated using the Keras library in Python. To ensure efficient training and convergence, we utilized the Adam optimizer with its default settings and employed binary cross-entropy as the loss function. To optimize the model's hyperparameters, including batch size, number of epochs, and number of neurons, we conducted a grid search over a range of values. Specifically, we explored learning rates of 0.001, 0.01, and 0.1; batch sizes of 16, 32, and 64; and numbers of epochs of 50, 100, and 200. The optimal combination was determined based on cross-validation performance, resulting in a batch size of 32, 200 epochs, and 50 neurons. Additionally, a dropout layer with a rate of 0.3 was introduced between the input layer and the LSTM network layer to enhance the model's generalization and robustness. Training involved multiple epochs with early stopping to prevent overfitting. The performance metrics used during training and validation included accuracy, sensitivity, specificity, and precision, ensuring a comprehensive evaluation of the model's effectiveness. Among these indicators, precision is particularly important for models taking samples with imbalanced classes as inputs.


https://doi.org/10.5607/en24028

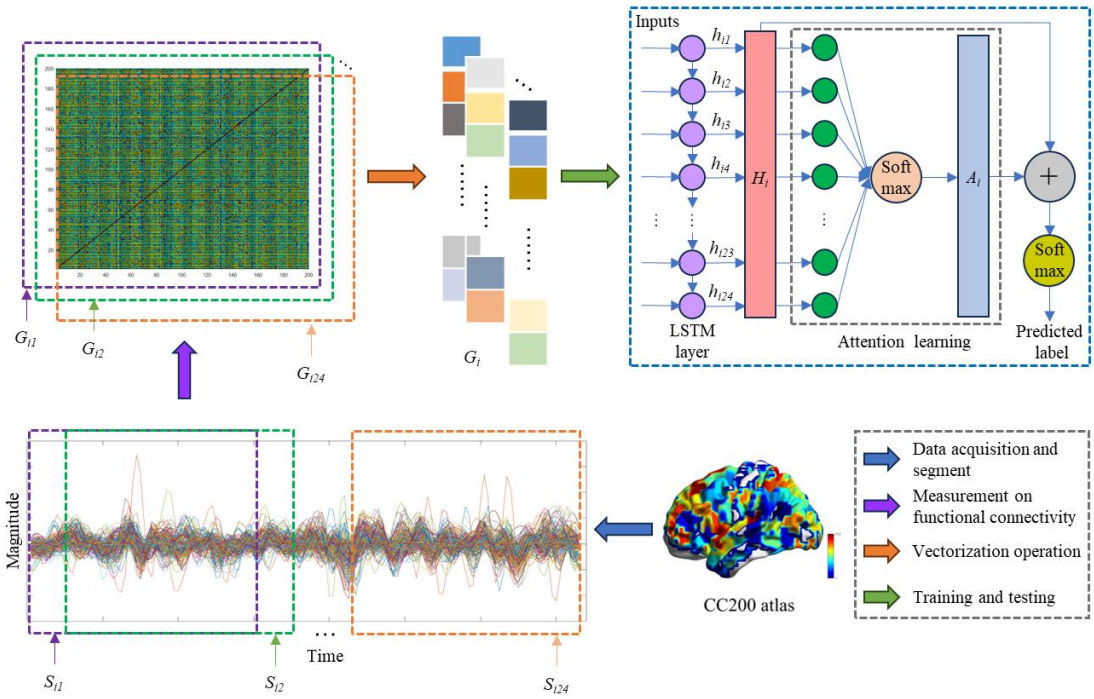


**Fig. 1.** A graphical representation of steps involved in the proposed classification model.

**Table 2.** Experimental results of different classification models

| Classifier | Accuracy (%) | Sensitivity (%) | Specificity (%) | Precision (%) |
|---|---|---|---|---|
| SVM | 68.9 | 57.1 | 79.6 | 71.6 |
| RF | 69.0 | 63.0 | 74.3 | 68.8 |
| LSTM | 73.6 | 70.0 | 76.9 | 73.2 |
| ATT | 74.9 | 70.0 | 79.3 | 75.5 |

ATT, attention learning.

## RESULTS AND DISCUSSION

### *Classification performance*

Based on intra-site cross-validation, the attention learning model achieved a classification accuracy of 74.9%, sensitivity of 70%, specificity of 79.3%, and precision of 75.5%. Notably, the specificity score was higher than the sensitivity score, which aligns with desired outcomes in clinical practice. This is because, in the general population, most individuals are not at risk of ASD, making the minimization of false positives crucial. These results demonstrate the potential of the proposed approach for identifying individuals with ASD.

To further validate the effectiveness of the attention learning model, we compared it with two traditional machine learning models—support vector machine (SVM) and random forest (RF)—and one deep learning model, a single LSTM network, serving as baseline classifiers. The traditional models utilized the feature vector derived from the upper triangle values of the functional connectivity matrix, excluding the diagonal values, with each element representing the Pearson correlation coefficient [13] between two ROIs in the brain. The LSTM network used the same samples as the attention learning model. To optimize performance, the parameters of these baseline classifiers were determined using a grid-based search strategy [24].

Table 2 presents the results of the experiments based on the three baseline classifiers and the attention learning model. Visual inspection reveals that the attention learning model outperformed the baseline classifiers, achieving the highest scores in accuracy, sensitivity, and precision. However, it scored lower in specificity compared to the SVM classifier, despite demonstrating superior overall classification performance. These comparison results confirm that our attention learning model is a feasible and effective method for identifying individuals at risk of ASD. In essence, the brain functional connectivity may manifest atypical temporal dependencies in patients with ASD, which our model is capable of capturing.

To further analyze the experimental results, we utilized the receiver operating characteristic (ROC) curve, with the area under the curve (AUC) serving as a metric for assessing the classifier's ability to accurately differentiate between TD individuals and patients with ASD. A higher AUC value indicates better classification performance. As depicted in Fig. 2a, the AUC values for the four

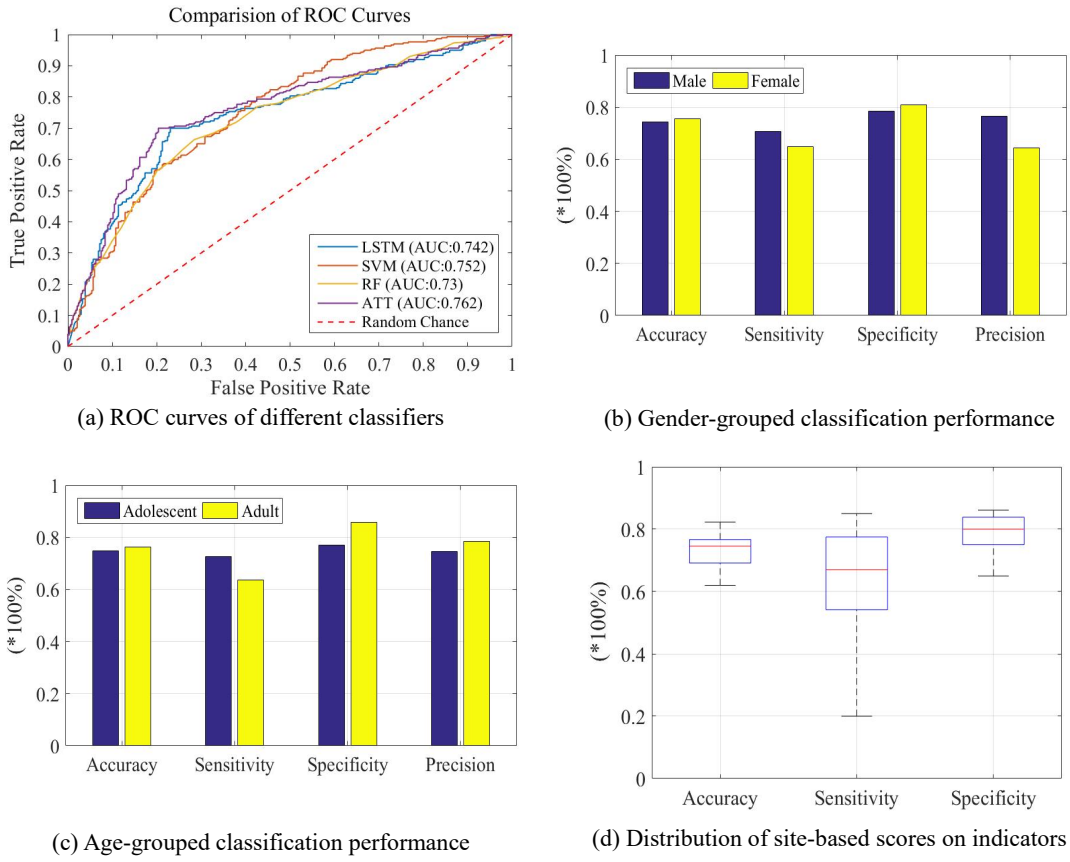


(a) ROC curves of different classifiers

(b) Gender-grouped classification performance

(c) Age-grouped classification performance

(d) Distribution of site-based scores on indicators

**Fig. 2.** Classification performance of proposed model.

classifiers were 0.752 (95% CI: 0.701~0.803) for SVM, 0.73 (95% CI: 0.678~0.782) for RF, 0.742 (95% CI: 0.691~0.793) for LSTM, and 0.762 (95% CI: 0.712~0.812) for the attention learning model. The CI denotes the confidence interval, which was calculated using the DeLong method [25]. This method provides a more comprehensive representation of the classification performance. Among these classifiers, the attention learning model achieved the highest AUC value, highlighting its potential utility in aiding the diagnosis of ASD.

While our model's accuracy is lower than that reported in some recent studies (e.g., Kong et al. [7]'s 90.39% and Guo et al. [8]'s 86.36%), it is important to note that these studies employed static functional connectivity methods with smaller sample sizes (172 and 110, respectively). In contrast, our study utilizes a dynamic functional connectivity approach with a larger sample size of 634 subjects. This larger sample size enhances the robustness and generalizability of our findings, allowing us to better capture the variability within the ASD population. And our dynamic approach could capture the temporal variability in brain connectivity patterns, whereas static methods assume a constant connectivity pattern over time and thus only provide a static snapshot of brain connectivity.

This temporal variability is essential for understanding the dynamic nature of brain function and its role in cognitive and behavioral processes. For instance, the decreased variability observed in the default-mode network (DMN) of individuals with ASD may reflect reduced flexibility in brain network dynamics, which is a hallmark of the disorder [26]. This reduced flexibility can impact the brain's ability to efficiently switch between different cognitive tasks and adapt to changing environmental demands. A recent study has demonstrated that certain dynamic states are linked to better executive functioning, such as cognitive flexibility and adaptability, which are often impaired in ASD [27]. These findings suggest that dynamic functional connectivity can reveal unique patterns of brain activity that are not apparent in static connectivity. Our positive experimental results, particularly in the context of a larger and more diverse dataset, further demonstrate the potential of our approach for identifying individuals with ASD.

 https://doi.org/10.5607/en24028

### *Reproduction performance*

Heterogeneity poses a significant challenge to the reproducibility of classification models, often manifesting in data acquisition protocols (e.g., scanner type), participant instructions (e.g., eyes open or closed), and subject recruitment strategies (e.g., age-range) [28]. To assess our model's robustness and reproducibility across different demographic groups, we conducted detailed analysis to determine whether our classification model is sensitive to variations in gender and age. It is important to note that we employed stratified sampling during the training process. Stratified sampling ensures that each batch of training data contains a representative distribution of samples, thereby reducing the impact of gender and age imbalance on model performance. This approach helps the model generalize better to diverse populations by ensuring it is trained on a more balanced dataset.

As shown in Fig. 2b, our attention learning model achieved a classification accuracy of over 74% in both male and female subjects. Notably, specificity scores were higher than sensitivity scores, aligning with clinical expectations. Precision was higher in the classification of male subjects compared to female subjects, which may be attributed to the greater number of male samples in the training procedure. Increasing the number of female training samples could potentially improve precision.

The results of age-grouped classification are presented in Fig. 2c. Consistent with a previous imaging study [5], we categorized subjects into adolescent (age<18) and adult (age>=18) groups. Our model performed well in classifying both groups, with accuracy, specificity, and precision scores all above 72%. Adolescents exhibited higher sensitivity scores compared to adults, suggesting that brain functional connectivity may exhibit more pronounced temporal dependencies in adolescent individuals with ASD.

From this analysis, we conclude that the current model demonstrates good reproducibility and robustness. Its classification performance appears to be less affected by the gender or age of subjects, indicating that the model is not overly sensitive to demographic variations and can generalize well to diverse populations. These findings further support the representativeness of our dataset and the applicability of our results to broader populations.

### *Generalization performance*

To investigate the generalization performance of the proposed approach, we conducted an analysis of site-based classification results, focusing on three key indicators: accuracy, sensitivity, and specificity. The precision indicator was excluded due to the limited number of samples from individual sites (e.g., 14 samples from CMU). As shown in Table 3, the attention learning model demonstrated promising classification performance across most sites. Except for CALTECH and SDSU, all sites achieved good accuracy above 70% and sensitivity above 60%. For specificity, scores exceeded 75% at all sites except STANFORD.

Notably, the highest accuracy (82.3%) and specificity (86.1%) were achieved by the USM-based classification, while STANFORD achieved the best sensitivity at 85%. The average scores for accuracy, sensitivity, and specificity were 73.0%, 61.7%, and 79.1%, respectively. Fig. 2d illustrates the distribution of site-based scores for these indicators. Both accuracy and specificity show a relatively narrow range of scores, with standard deviations of 5.8% and 6.3%, respectively. In contrast, sensitivity scores ranged from 20% to 85%, indicating greater variability. This dispersion may be attributed to the small number of subjects at some sites, such as CALTECH and SDSU. Increasing the number of subjects at these sites could improve classification performance. Overall, our proposed approach demonstrates robust generalization performance and holds promise for broader applications. This supports the notion that our findings are applicable across different clinical and demographic settings.

### *Discriminative functional connectomes*

Based on heterogeneous rs-fMRI data, our proposed model accurately differentiated between TD individuals and patients with ASD. A key challenge in the modeling process was identifying discriminative features that not only contribute to accurate classification but also hold promise for identifying objective biomarkers of ASD. To address this, we analyzed the weights of the optimal model to discover discriminative functional connectomes. It is important to note that the sign of the weights is not significant; only the magnitude is considered. Specifically, weights with magnitudes more than 2 standard deviations away from the mean are deemed significant.

Fig. 3 illustrates the most discriminative connectomes grouped by layers of cell state and output gate, which together determine

**Table 3.** Site-based classification performance

| SITE_ID | Count | Accuracy (%) | Sensitivity (%) | Specificity (%) |
|---|---|---|---|---|
| CALTECH | 21 | 62.0 | 20.0 | 83.3 |
| CMU | 14 | 76.7 | 60.0 | 80.0 |
| NYU | 182 | 73.6 | 60.7 | 83.5 |
| SDSU | 29 | 66.0 | 36.7 | 85.0 |
| STANFORD | 40 | 75.0 | 85.0 | 65.0 |
| TRINITY | 47 | 70.2 | 67.0 | 75.0 |
| UM | 145 | 76.8 | 76.8 | 75.0 |
| USM | 101 | 82.3 | 79.5 | 86.1 |
| YALE | 55 | 74.5 | 69.3 | 78.7 |
| AVERAGE | -- | 73.0 | 61.7 | 79.1 |

Values in count column stands for number of involved subjects in site.

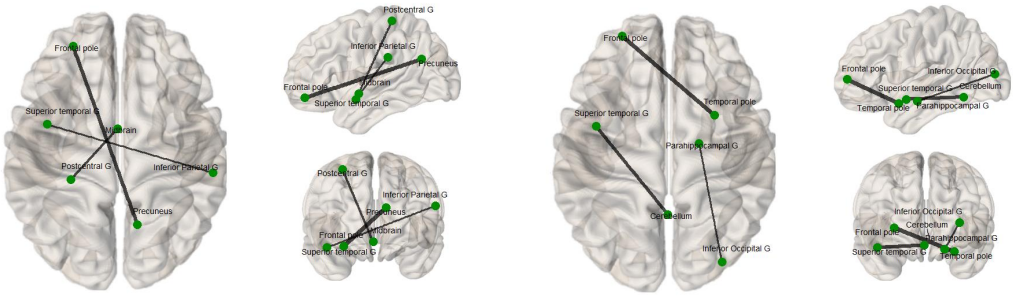


(a) Cell state (b) Output gate

**Fig. 3.** Discriminative functional connectomes.

the output of each module in the LSTM network. The thickness of the lines in the figure indicates the magnitude of the weights, with thicker lines representing greater weights and stronger discriminative ability. Compared to TD individuals, patients with ASD may exhibit atypical temporal dependencies in these connectomes, which could manifest as dynamic changes over time. Importantly, the cell state layer highlights connectomes (Fig. 3a) that may reflect long-term variations, while the output gate emphasizes connectomes (Fig. 3b) that may reflect short-term variations.

## CONCLUSION

In this study, we investigated the temporal dependencies of brain functional connectivity to differentiate between TD individuals and patients with ASD. We employed an attention learning framework based on the LSTM network, which processes sequences of segments as inputs. This approach enables the model to capture both the static characteristics of functional connectivity within segments and the dynamic changes over time from the global sequence. Using heterogeneous rs-fMRI data, our attention learning model achieved an accuracy of 74.9% and precision of 75.5%, outperforming baseline classifiers, including traditional machine learning models (SVM and RF) and a single LSTM network. The higher AUC value (0.762) further supports the model's effectiveness. Our analysis of group-based and site-based classification results demonstrated the model's reproducibility and generalizability. Notably, the model's performance appears to be less affected by the subjects' gender or age. The optimal model's weights highlighted discriminative functional connectomes that may reflect atypical temporal dependencies in individuals with ASD.

Our study has several limitations that will guide future research. One critical limitation is the variability in sample sizes across sites, with some sites having as few as 14 subjects (i.e., CMU). This can introduce significant variability in site-based results and limit the generalizability of our findings. To address this, we have outlined future research directions, including the potential for expanding our sample size by incorporating additional datasets or using more inclusive preprocessing methods. This would allow for a more diverse and representative sample, thereby improving the generalizability of future studies. Additionally, advanced statistical methods or machine learning techniques that can explicitly model inter-site variability should be considered to improve the robustness and generalizability of the results. It is important to note that our study's design primarily focused on validating the methodology rather than its clinical implementation. Future studies will address the model's clinical utility using separate training and testing datasets from independent cohorts.

Another limitation is the lack of detailed biological interpretation of the discriminative functional connectomes identified. While our model captures atypical temporal dependencies in brain connectivity, translating these findings into specific biological mechanisms requires additional neurobiological data and analyses. Future work should focus on integrating our findings with other imaging modalities (e.g., structural MRI, diffusion tensor imaging) and clinical assessments to provide a more comprehensive understanding of ASD pathophysiology. Collaborations with neurobiologists and clinicians could help bridge the gap between functional connectivity patterns and their biological significance.

In addition, the comparative analysis was based only on traditional classifiers (SVM, RF) and a single LSTM network. To provide a more comprehensive evaluation of our model's performance, future work will include more advanced deep learning architectures, such as 3D convolutional neural networks (CNNs) and graph neural networks (GNNs), which have shown promise in recent ASD classification studies. This will further validate the superiority of our approach over existing methods.

 https://doi.org/10.5607/en24028

## ACKNOWLEDGEMENTS

This work was supported by the National Natural Science Foundation of China (Grant No. 62306108), the Natural Science Foundation of Hubei Province in China (Grant No. 2023AFB042), the Natural Science Fund Project of Hubei Province (Grant No. 2023AFB585), and the Scientific Research Foundation for the Hubei University of Arts and Science (Grant No. 2059204).

## CONFLICT OF INTEREST

The authors declare no potential conflicts of interest.

## REFERENCES

1. Maqbool S, Zahra W, Ali A, Azhar H, Farid A, Ullah E, Brown N (2023) Eclectic approach in children with autism spectrum disorder: an experience from a developing country. Adv Neurodev Disord 7:88-93.
2. Rellini E, Tortolani D, Trillo S, Carbone S, Montecchi F (2004) Childhood autism rating scale (CARS) and autism behavior checklist (ABC) correspondence and conflicts with DSM-IV criteria in diagnosis of autism. J Autism Dev Disord 34:703-708.
3. Geier DA, Kern JK, Geier MR (2013) A comparison of the autism treatment evaluation checklist (ATEC) and the childhood autism rating scale (CARS) for the quantitative evaluation of autism. J Ment Health Res Intellect Disabil 6:255-267.
4. Subbaraju V, Suresh MB, Sundaram S, Narasimhan S (2017) Identifying differences in brain activities and an accurate detection of autism spectrum disorder using resting state functional-magnetic resonance imaging: a spatial filtering approach. Med Image Anal 35:375-389.
5. Huang ZA, Zhu Z, Yau CH, Tan KC (2021) Identifying autism spectrum disorder from resting-state fMRI using deep belief network. IEEE Trans Neural Netw Learn Syst 32:2847-2861.
6. Cao M, Yang M, Qin C, Zhu X, Chen Y, Wang J, Liu T (2021) Using DeepGCN to identify the autism spectrum disorder from multi-site resting-state data. Biomed Signal Process Control 70:103015.
7. Kong Y, Gao J, Xu Y, Pan Y, Wang J, Liu J (2019) Classification of autism spectrum disorder by combining brain connectivity and deep neural network classifier. Neurocomputing 324: 63-68.
8. Guo X, Dominick KC, Minai AA, Li H, Erickson CA, Lu LJ (2017) Diagnosing autism spectrum disorder from brain resting-state functional connectivity patterns using a deep neural network with a novel feature selection method. Front Neurosci 11:460.
9. Chen H, Duan X, Liu F, Lu F, Ma X, Zhang Y, Uddin LQ, Chen H (2016) Multivariate classification of autism spectrum disorder using frequency-specific resting-state functional connectivity--a multi-center study. Prog Neuropsychopharmacol Biol Psychiatry 64:1-9.
10. Deng L, Yu D (2014) Deep learning: methods and applications. Now Found Trend Signal Process 7:197-387.
11. Deng X, Zhang J, Liu R, Liu K (2022) Classifying ASD based on time-series fMRI using spatial-temporal transformer. Comput Biol Med 151:106320.
12. Heinsfeld AS, Franco AR, Craddock RC, Buchweitz A, Meneguzzi F (2017) Identification of autism spectrum disorder using deep learning and the ABIDE dataset. Neuroimage Clin 17:16-23.
13. Eslami T, Mirjalili V, Fong A, Laird AR, Saeed F (2019) ASD-DiagNet: a hybrid learning approach for detection of autism spectrum disorder using fMRI data. Front Neuroinform 13:70.
14. Di Martino A, Yan CG, Li Q, Denio E, Castellanos FX, Alaerts K, Anderson JS, Assaf M, Bookheimer SY, Dapretto M, Deen B, Delmonte S, Dinstein I, Ertl-Wagner B, Fair DA, Gallagher L, Kennedy DP, Keown CL, Keysers C, Lainhart JE, Lord C, Luna B, Menon V, Minshew NJ, Monk CS, Mueller S, Müller RA, Nebel MB, Nigg JT, O'Hearn K, Pelphrey KA, Peltier SJ, Rudie JD, Sunaert S, Thioux M, Tyszka JM, Uddin LQ, Verhoeven JS, Wenderoth N, Wiggins JL, Mostofsky SH, Milham MP (2014) The autism brain imaging data exchange: towards a large-scale evaluation of the intrinsic brain architecture in autism. Mol Psychiatry 19: 659-667.
15. Loomes R, Hull L, Mandy WPL (2017) What is the male-to-female ratio in autism spectrum disorder? A systematic review and meta-analysis. J Am Acad Child Adolesc Psychiatry 56:466-474.
16. Craddock RC, James GA, Holtzheimer PE 3rd, Hu XP, Mayberg HS (2012) A whole brain fMRI atlas generated via spatially constrained spectral clustering. Hum Brain Mapp 33:1914-1928.
17. Esteban O, Markiewicz CJ, Blair RW, Moodie CA, Isik AI, Erramuzpe A, Kent JD, Goncalves M, DuPre E, Snyder M, Oya H, Ghosh SS, Wright J, Durnez J, Poldrack RA, Gorgolewski KI (2019) fMRIPrep: a robust preprocessing pipeline for functional MRI. Nat Methods 16:111-116.
18. Campo F, Retico A, Calderoni S, Oliva P (2023) Multi-site MRI data harmonization with an adversarial learning approach: implementation to the study of brain connectivity in

autism spectrum disorders. Appl Sci 13:6486.
19. BenYahmed Y, Bakar AA, RazakHamdan A, Ahmed A, Abdullah SMS (2015) Adaptive sliding window algorithm for weather data segmentation. J Theor Appl Inf Technol 80:322-333.
20. Preti MG, Bolton TA, Van De Ville D (2017) The dynamic functional connectome: state-of-the-art and perspectives. Neuroimage 160:41-54.
21. Thompson WH, Fransson P (2015) The frequency dimension of fMRI dynamic connectivity: network connectivity, functional hubs and integration in the resting brain. Neuroimage 121:227-242.
22. Ghojogh B, Ghodsi A (2023) Recurrent neural networks and long short-term memory networks: tutorial and survey. arXiv 2304.11461.
23. Abraham A, Milham MP, Di Martino A, Craddock RC, Samaras D, Thirion B, Varoquaux G (2017) Deriving reproducible biomarkers from multi-site resting-state data: an autism-based example. Neuroimage 147:736-745.
24. Syarif I, Prugel-Bennett A, Wills G (2016) SVM parameter optimization using grid search and genetic algorithm to improve classification performance. Telecommun Comput Electron Control 14:1502-1509.
25. Sun X, Xu W (2014) Fast implementation of DeLong's algorithm for comparing the areas under correlated receiver operating characteristic curves. IEEE Signal Process Lett 21:1389-1393.
26. Asadi N, Olson IR, Obradovic Z (2021) The backbone network of dynamic functional connectivity. Netw Neurosci 5:851-873.
27. Fu Z, Sui J, Iraji A, Liu J, Calhoun VD (2025) Cognitive and psychiatric relevance of dynamic functional connectivity states in a large (N>10,000) children population. Mol Psychiatry 30:402-413.
28. Yan CG, Craddock RC, Zuo XN, Zang YF, Milham MP (2013) Standardizing the intrinsic brain: towards robust measurement of inter-individual variation in 1000 functional connectomes. Neuroimage 80:246-262.